Applied Catalysis B: Environmental 142–143 (2013) 169–177

Contents lists available at SciVerse ScienceDirect

Applied Catalysis B: Environmental

journal homepage: www.elsevier.com/locate/apcatb

Role of CO_2 on CO preferential oxidation over CuO/CeO_2 catalyst

A. Di Benedetto[a], G. Landi[b,*], L. Lisi[b], G. Russo[a]

[a] DICMAPI – University of Naples Federico II, P.le Tecchio 80, 80125 Naples, Italy
[b] Institute of Researches on Combustion-CNR, P.le Tecchio 80, 80125 Naples, Italy

ARTICLE INFO

Article history:
Received 29 January 2013
Received in revised form 12 April 2013
Accepted 1 May 2013
Available online 16 May 2013

Keywords:
CO-PROX
CuO/CeO_2 catalysts
CO_2 inhibition
TPD
Kinetic model

ABSTRACT

The inhibiting effect of the presence of CO_2 (15 vol.%) in the reaction mixture of CO-PROX reaction on the performance of CuO/CeO_2 catalysts has been investigated; CO_2 depresses CO oxidation up to 160 °C, its effect being negligible at higher temperatures. The CO_2 coverage of both ceria support and catalysts has been quantitatively determined by CO_2 TPD experiments and the distribution of adsorbing sites has been modeled. Two sites for CeO_2 (one modified by the strong interaction between Ce and Cu when copper is added) and an additional site associated to less interacting copper for CuO/CeO_2 catalysts have been identified by the mathematical model. Although ceria gives a large contribution to CO_2 adsorption, the sites present in larger amount rapidly desorb CO_2 in the typical temperature range of CO-PROX reaction (80–150 °C), especially when copper modification induces a decrease of desorption activation energy, thus suggesting that these centres are involved in CO oxidation. Adsorption sites attributed to copper less interacting with the support still keep a fraction of adsorbed CO_2 in this temperature range and the higher selectivity suggested that they can be mainly related to the H_2 oxidation activity.

1. Introduction

The polymeric membrane fuel cell (PEMFC) represents an attractive technological solution for the generation of power at small scale due to the compactness, modularity, efficiency and environmental impact.

The hydrogen stream feeding the fuel cell, produced through a reforming process and subsequent stages of water-gas-shift (WGS), can still contain 0.5–1 vol.% CO that poisons the Pt catalyst at the anode of the fuel cell. It is then necessary to reduce the CO concentration to an acceptable level of 10–50 ppm.

A promising technological solution is based on the process of catalytic preferential oxidation of CO (CO-PROX) [1–6].

A proper catalyst for the CO-PROX process must ensure high activity, stability and selectivity in the temperature range 80–200 °C. This temperature range depends on the upstream (water gas shift) and downstream (PEMFC) stages of the process: the low temperature WGS stage working at 200 °C and the PEMFC working at 80 °C.

Copper/ceria based catalysts have been proposed as alternative systems to noble metals for CO-PROX reaction since they show performances even higher than those reported for the more expensive noble metals [7–10].

Liu et al. [11,12] related the activity of these catalysts towards CO oxidation to the presence of Cu^{+1} species formed by the interaction between copper and cerium oxide. The presence of Cu^{+1} was also shown by many authors [7,13–16].

The reaction path is assumed to follow a redox mechanism, involving the change of the oxidation state of both copper ($Cu^{2+} \leftrightarrow Cu^{1+}$) and cerium ($Ce^{4+} \leftrightarrow Ce^{3+}$) [10,17–21]. According to this hypothesis, the active sites for the CO oxidation reaction were identified as the interface sites between copper oxide and the support.

Most of these works has been conducted on mixtures composed exclusively of CO and H_2, and then under conditions far from the real ones. Actually, the average composition of the stream coming out from the steam reforming and WGS processes is: H_2 (50–75%), CO (0.5–1%), CO_2 (10–20%) and H_2O (5–10%).

The inhibiting role of both H_2O and CO_2 on the CO-PROX over $CuO–CeO_2$ catalysts have been shown [8,9,14,22]. In the typical temperature range of the CO-PROX process it has been demonstrated that, in contrast with noble metal-based systems [2,23], copper/ceria catalyst are not able to activate both WGS and r-WGS. Consequently, the effect of CO_2 and H_2O has to be related to the chemical/physical interaction with the catalyst.

Mariño et al. [24] proposed that the decrease of CO oxidation activity with increasing CO_2 content in the stream up to 15 % could be related to the competitive adsorption of CO_2 on the active copper sites and/or to the inhibition of oxygen mobility upon formation of carbonates on the ceria support. In agreement with Mariño et al.

* Corresponding author. Tel.: +39 0817682235.
E-mail address: landi@irc.cnr.it (G. Landi).

0926-3373/$ – see front matter © 2013 Elsevier B.V. All rights reserved.
http://dx.doi.org/10.1016/j.apcatb.2013.05.001

[24], Gamarra and Martinez-Arias [25] addressed the deactivating effect of CO_2 to the hindering of interfacial redox activity caused by the formation of carbonate-type species (hydrogen carbonate, bidentate carbonate). They also reported that adsorption of water and hydroxyl formation prevents the access of reactant molecules to the interfacial sites. Nevertheless, they showed that the inhibiting effect of water is lower than that induced by CO_2 concluding that carbonate species hinders more strongly the interfacial redox activity. Lee and Kim [26] performed a kinetic study of the H_2 and CO oxidation over CuO/CeO_2 catalyst. They found that CO and H_2 oxidation reaction rates are independent suggesting that sites for CO and H_2 adsorption on the $CuO\text{-}CeO_2$ are different: Cu^+-carbonyl sites are active for CO oxidation while Cu^0 sites for H_2 oxidation. They also tested the role of CO_2 and H_2O highlighting that the oxidation rates of both CO and H_2 have negative reaction orders with respect to the partial pressures of CO_2 and H_2O. On the contrary, Kydd et al. [27] reported that on CuO/CeO_2 catalysts prepared by flame spray pyrolysis CO and H_2 compete for the same sites, selectivity towards CO oxidation being assured by carbonyl stabilization preventing H_2 adsorption.

Park et al. [28] compared the catalytic activity with the CO_2 and H_2O TPD results. They suggested that CO_2 and H_2O compete with CO for the adsorption on the same active sites relating the CO oxidation activity with the desorption temperature of CO_2 and H_2O. The adsorption of CO_2 was investigated also by Avgouropoulos and Ioannides [29] by TPD experiments on $CuO\text{-}CeO_2$ catalysts prepared by combustion synthesis showing that CO_2 is desorbed giving a tailed peak up to 300–400 °C related to carbonates decomposition.

In this work the role of CO_2 on the activity and selectivity was quantified by assessing the extent of adsorption of CO_2 over a CuO-based catalyst supported on CeO_2.

To this end we performed activity tests measuring the CO conversion and selectivity at different temperatures. The results have been correlated to CO_2 temperature programmed desorption (TPD) runs over both the support (CeO_2) and the catalyst (CuO/CeO_2), at different CuO content.

A model of CO_2 TPD was developed highlighting the relation between the CO_2 adsorption and CO-PROX activity and selectivity.

2. Materials and methods

2.1. Catalyst preparation and characterization

A commercial CeO_2 supplied by Grace was used as support. The CuO/CeO_2 catalysts were prepared by wet impregnation of the support with copper acetate ($(CH_3COO)_2Cu{\cdot}H_2O$; Aldrich, assay 99.8%) as copper precursor using a rotating evaporator at 50 °C, 90 mbar and 120 rpm. A $(CH_3COO)_2Cu{\cdot}H_2O$ amount to obtain the desired nominal CuO content was dissolved in aqueous solution. The sample was then dried overnight at 120 °C and subsequently calcined at 450 °C under dry air flow (5 N l/h) for 3 h. Catalysts with nominal CuO weight percentage equal to 0.5, 4 and 8 were prepared.

The copper concentrations were determined by an Agilent 7500 ICP-MS. The values of surface area were determined by BET method adsorbing N_2 at 77 K using a Quantachrome Autosorb 1-C.

CO_2 TPD experiments were carried out using a Micromeritics Autochem II 2020 analyzer equipped with a TC detector. About 100 mg sample was pre-treated 1 h at 450 °C in flowing air and then contacted for 45 min at room temperature with a 15% CO_2/He mixture. After 30 min He purging the sample was heated 10 °C min^{-1} up to 300 °C.

2.2. Experimental set-up

The lab-scale set-up used for CO-PROX experiments can be ideally divided into three sections: (i) gas feed preparation and control, (ii) reaction zone and (iii) gas analysis. O_2, N_2, CO_2 at high purity, 5%CO/N_2 from gas cilynders and high purity H_2 from H_2 generator (CLAIND HG2200) have been independently controlled through mass flow controllers (Brooks 5850S). Besides, a pressure transducer is placed just downstream the gasses mixing point thus allowing the on-line monitoring of the pressure. The reactor can be by-passed using a four-way valve; in this way the analysis of both reacting mixture and reactor off products can be performed by the same analysis system.

The powder catalyst (300 mg) with a particle size of 200–400 μm was placed in a tubular quartz reactor. A thermocouple placed inside a tube co-axial with the reactor provided the measurement of the catalyst temperature. The reactor is externally heated by an electric tubular furnace (Lenton) provided with a PID-type controller.

An ice bath based condenser and a $CaCl_2$ trap are used in order to dry the gaseous flow downstream to the reactor; the dried flow is analyzed with a Fisher-Rosemount NGA2000 continuous analyzer monitoring the main gas species (CO_2 and CO by infrared detectors, O_2 by a paramagnetic detector and H_2 by a thermoconducibility detector) and equipped with a cross sensitivity correction.

Catalytic tests were conducted at fixed flow rate (20 l(STP)/h) corresponding to a contact time of 0.054 g s/cm^3. Hydrogen, carbon monoxide and oxygen concentrations were fixed at 50 vol.%, 0.5 vol.% and 0.9 vol.% respectively, while two carbon dioxide (0 vol.% and 15 vol.%) concentrations were used. Reaction temperature was varied between 60 °C and 220 °C, thus covering the whole temperature range of interest for CO-PROX. Even if water is generally present in the gaseous stream incoming into a CO-PROX reactor, in this study it was not added to the reaction mixture in order to avoid the overlapping of the effect of carbon dioxide and water on the catalytic performance.

Mass balances were always closed within ±4%. Reactants conversions and selectivity of oxygen reacting with carbon monoxide were calculated according to the following equations:

$$x_{CO} = \frac{CO^{IN} - CO^{OUT}}{CO^{IN}} \quad (1)$$

$$x_{O_2} = \frac{O_2^{IN} - O_2^{OUT}}{O_2^{IN}} \quad (2)$$

$$x_{H_2} = \frac{H_2^{IN} - H_2^{OUT}}{H_2^{IN}} \quad (3)$$

$$s_{CO} = \frac{\Delta O_2^{CO}}{\Delta O_2^{CO} + \Delta O_2^{H_2}} = 0.5 \cdot \frac{CO^{IN} - CO^{OUT}}{O_2^{IN} - O_2^{OUT}} \quad (4)$$

where x_{CO}, x_{O_2}, x_{H_2} and s_{CO} are, respectively, the CO, O_2 and H_2 conversions and the O_2 selectivity to CO_2 and $\Delta O_2{}^{CO}$ and $\Delta O_2{}^{H_2}$ the oxygen moles consumed for CO and H_2 oxidation respectively.

2.3. Model

In order to get insights into the nature of the catalytic sites involved in the CO_2 adsorption/desorption, we developed a model of CO_2 TPD.

It is based on the kinetic model on the Polanyi–Wigner equation under the Redhead approximation which states that the catalytic sites do not interact.

From the TPD signals of the materials three peaks establish.

We then assumed that CO_2 adsorb over three catalytic sites, giving rise to the following desorption step:

$$\left(CO_2 - \sigma_1 \xrightarrow{k_1} CO_2 + \sigma_1\right) \quad (5)$$

$$\left(CO_2 - \sigma_2 \xrightarrow{k_2} CO_2 + \sigma_2\right) \quad (6)$$

$$\left(CO_2 - \sigma_3 \xrightarrow{k_3} CO_2 + \sigma_3\right) \quad (7)$$

The rates of step 1–3 are:

$$r_1 = k_1 \vartheta_1^{n1} \quad (8)$$

$$r_2 = k_2 \vartheta_2^{n2} \quad (9)$$

$$r_3 = k_3 \vartheta_3^{n3} \quad (10)$$

where θ_1, θ_2 and θ_3 are the fractions of site (CO_2-σ_1), (CO_2-σ_2) and (CO_2-σ_3) respectively with respect to the total number of sites.

We assumed that both the desorption activation energy (E_{des}) and the frequency factor (k^0) are not dependent on the adsorption degree (Redhead Approximation). Accordingly, the kinetic constants are evaluated as follows:

$$k_1 = k_1^0 \exp\left(-E_{des1}/RT\right) \quad (11)$$

$$k_2 = k_2^0 \exp\left(-E_{des2}/RT\right) \quad (12)$$

$$k_3 = k_3^0 \exp\left(-E_{des3}/RT\right) \quad (13)$$

The unsteady balance equations on the fraction (θ_1, θ_2 and θ_3) read:

$$\frac{d\theta_1}{dt} = -k_1^0 \exp\left(-E_{des1}/RT\right) \vartheta_1^{n1} \quad (14)$$

$$\frac{d\theta_2}{dt} = -k_2^0 \exp\left(-E_{des2}/RT\right) \vartheta_2^{n2} \quad (15)$$

$$\frac{d\theta_3}{dt} = -k_3^0 \exp\left(-E_{des3}/RT\right) \vartheta_3^{n3} \quad (16)$$

The initial conditions are:

$$t = 0 \quad \theta_1 = \theta_1^0 \quad (17)$$

$$t = 0 \quad \theta_2 = \theta_2^0 \quad (18)$$

$$t = 0 \quad \theta_3 = \theta_3^0 \quad (19)$$

The CO_2 molar balance equation is the following, assuming perfect mixing of the reactor and pseudo-steady state conditions:

$$\frac{1}{C^0}\frac{dC_{CO_2}}{dt} - \frac{C_{CO_2}}{C^0\tau} = k_1^0 \exp\left(-\frac{E_{des1}}{RT}\right) \vartheta_1^{n1} + k_2^0 \exp\left(-\frac{E_{des2}}{RT}\right) \vartheta_2^{n2} + k_3^0 \exp\left(-\frac{E_{des3}}{RT}\right) \vartheta_3^{n3} \quad (20)$$

where C is the total gas concentration in mol g^{-1} and τ is the residence time (s).

The initial condition of the CO_2 molar balance is the following:

$$t = 0 \quad C_{CO_2} = 0 \quad (21)$$

The temperature increase in the TPD experiment is linear with time (t):

$$T = T^0 + \beta t \quad (22)$$

where $\beta = 10\,^{\circ}C\,min^{-1}$.

Table 1
Surface area and amount of CO_2 desorbed in the TPD experiments for support and catalysts.

Sample	Surface area ($m^2\,g^{-1}$)	Desorbed CO_2 ($\mu mol\,g^{-1}$)	Desorbed CO_2 ($\mu mol\,m^{-2}$)
CeO_2	56	300	5.36
0.5% CuO/CeO_2	56	324	5.79
4% CuO/CeO_2	50	296	5.92
8% CuO/CeO_2	47	325	6.91

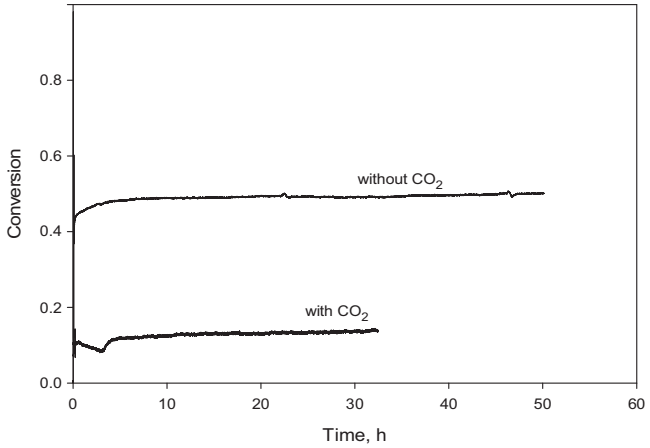

Fig. 1. CO conversion as a function of the time-on-stream for 4% CuO/CeO_2 catalyst at 90 °C. $\tau = 0.054\,g\,s/cm^3$; $CO/O_2/H_2/(CO_2) = 0.5/0.9/50/(15)$.

Eqs. (14)–(16) and (20) with the initial conditions ((17)–(19) and (21)) were solved by means of a Runge–Kutta method.

3. Results

The values of copper content determined by ICP analysis were close to the theoretical values. A significant surface area reduction with respect to that of the support (Table 1) can be noticed only at high copper loading when formation of small CuO crystallites was detected [30].

3.1. Activity tests

CuO/CeO_2 catalysts may show deactivation with time-on-stream due to different reasons, such as accumulation of hydroxyl species and/or carbonates on active interfacial sites and/or to copper sintering [7].

In order to verify the possible occurrence of deactivation we performed long-run tests at relatively low temperature (about 90 °C) for ensuring a CO conversion much lower than 100% (about 60%) to easily detect changes with time-on-stream related to deactivation [7]. In Fig. 1 CO conversion is shown as a function of time-on-stream in the absence and in the presence of 15 vol.% CO_2 over the 4% CuO/CeO_2 catalyst. Although significantly lower, a stable CO conversion was observed also in the presence of CO_2. No sign of deactivation can be detected after several hours on stream in both cases, thus suggesting that the catalyst is stable and that no continuous accumulation of any species (hydroxyls or carbonates) occurs during the reaction. In other words, the effect of CO_2 should be immediate and further exposure to CO_2 does not cause a progressive deactivation. The same occurs for the CO_2-free reaction mixture. Since CO conversion at 90 °C in presence of CO_2 is quite low (about 13%), test at higher temperature (120 °C) was also performed so to reach CO conversion up to about 40%. In agreement with the results obtained at 90 °C also the long-run at 120 °C (not reported) did not show any catalyst deactivation. Furthermore, the

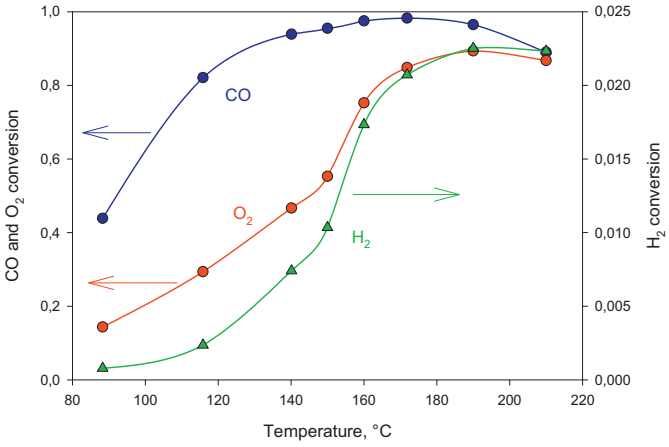

Fig. 2. CO, O_2 and H_2 conversions as a function of catalyst temperature for 4% CuO/CeO_2 catalyst; $\tau = 0.054$ g s/cm^3; $CO/O_2/H_2 = 0.5/0.9/50$.

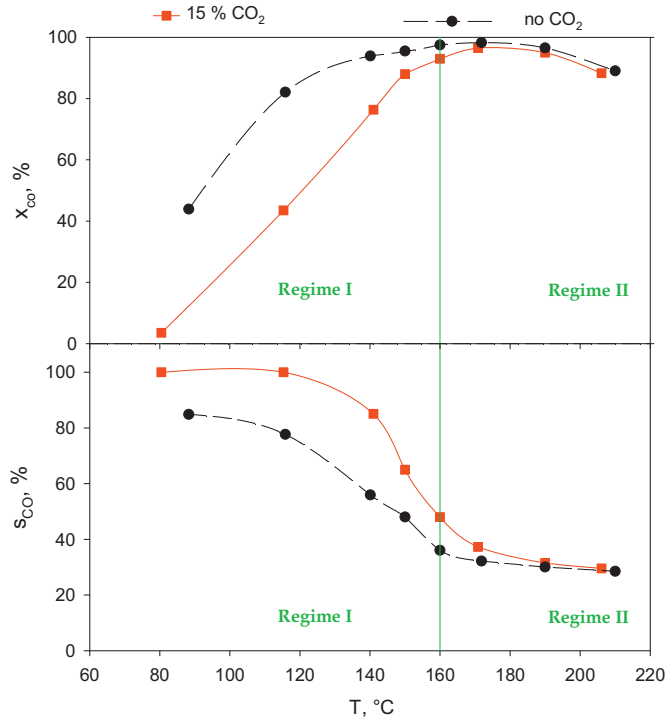

Fig. 3. Effect of CO_2 addition on CO-PROX performance of 4%Cu/CeO_2 catalyst: CO conversion (top); CO selectivity (bottom). $\tau = 0.054$ g s/cm^3; $CO/O_2/H_2 = 0.5/0.9/50$.

lower but stable CO conversion in the presence of CO_2, depending on the reaction temperature, suggests that a rapid equilibrium between adsorbed gaseous species takes place.

In Fig. 2 the conversions of CO, O_2 and H_2 are plotted as a function of the catalyst temperature.

It is found that CO reaction starts at temperature lower than 80 °C, while the H_2 oxidation ignites at temperature higher than 130 °C. At the H_2 ignition temperature a significant increase of the slope of the oxygen conversion is found.

In Fig. 3 the CO conversion and selectivity are plotted as a function of the catalyst temperature as obtained in the absence and in the presence of CO_2 (15 vol.%).

From these results two different operating regimes may be distinguished.

The first regime (I) occurs in the low temperature range ($T < 160$ °C) where CO conversion and selectivity are both affected by the presence of CO_2. In the second regime (II) ($T > 160$ °C), the performances of the CuO/CeO_2 catalyst towards CO-PROX seem not affected by the presence of CO_2.

It is worth noting that in regime I the presence of CO_2 decreases the CO conversion but increases the selectivity.

In Fig. 4 the CO conversion and selectivity are plotted as a function of the temperature as obtained over CuO/CeO_2 at two different CuO contents (0.5 and 4 wt.%), in the absence and in the presence of CO_2 (15 vol.%). No detectable activity was reported for CeO_2 support also under CO_2-free conditions at 100 °C [31]. Accordingly, it has been reported that CO activation on pure ceria occurs at temperatures higher than 200 °C [11]. Anyhow in this work the negligible activity of the support was verified up to 200 °C.

On increasing the Cu content (from 0.5 to 4%) CO conversion increases. This result confirms previous findings which report that the activity increases up to 4 wt.% CuO [31]. In the same paper it was reported that a further increase of the CuO content did not change the catalytic activity, additional copper seeming inactive towards CO activation [31].

On both catalysts, the effect of CO_2 on CO conversion and selectivity is negligible at high temperature (higher than 160 °C). At lower temperature, the CO_2 co-feeding reduces the CO conversion. Also the selectivity seems to be affected by the presence of CO_2 only at low temperature ($T < 160$ °C). Surprisingly, the role of CO_2 is to increase the CO selectivity in the low temperature rage. It should be underlined that the catalytic activity at high temperature seems quite unaffected by copper content. Nevertheless, as stated above, copper is necessary to obtain significant CO conversion also at high temperature, pure ceria activity being negligible.

In order to get insights into the reasons of this behavior, we performed CO_2 temperature programmed desorption (TPD) over the support CeO_2 and CuO/CeO_2 at different CuO content (0.5, 4 and 8 wt.%) and developed a model of CO_2 desorption.

3.2. TPD

In Fig. 5 the experimental TPD curves are plotted in terms of CO_2 desorbed as function of time over the CeO_2 support and the CuO/CeO_2 catalysts at different values of the CuO content (0.5, 4 and 8 wt.%). The CO_2 sorption capacity of the support is comparable to that of the CuO/CeO_2 catalysts suggesting a significant contribution of ceria in the CO_2 surface interaction.

In Table 1 the amount of CO_2 desorbed from all samples, evaluated from the integration of TPD profiles, is given. For all samples, support included, a CO_2 amount of roughly 300 μmol g^{-1} was evaluated by the integration of TPD curves with no apparent trend with respect to copper loading. Nevertheless, if the CO_2 amount is related to the surface area it increases with CuO loading indicating that copper provides additional adsorption sites. Indeed, the addition of copper reduces the original surface area of the support but not appreciably its sorption capacity. Whatever the nature of the new adsorption sites associated to copper (new copper species or modification of CeO_2 sites) their contribution must be larger than that of CeO_2 sites possibly blocked by copper oxide impregnation.

Further CO_2 TPD experiments were carried out on 4% CuO/CeO_2 catalysts after 30 min in situ isothermal reduction of the sample at 80 and 130 °C respectively (heating rate 5 °C min^{-1}) in H_2/Ar mixture. Although the catalyst undergoes a reduction, estimated as H_2/Cu ratio, of 0.024 and 0.69 at 80 and 130 °C respectively, the subsequent CO_2 TPD profiles are perfectly overlapped suggesting that CO_2 adsorption is not selective towards oxidized or reduced copper and/or cerium. As a consequence the following discussion will be focused on the TPD curves of oxidized catalysts.

The temperature range in which CO_2 is desorbed from the catalyst is 80–300 °C and it is coincident with the range in which the CO-PROX reaction is active.

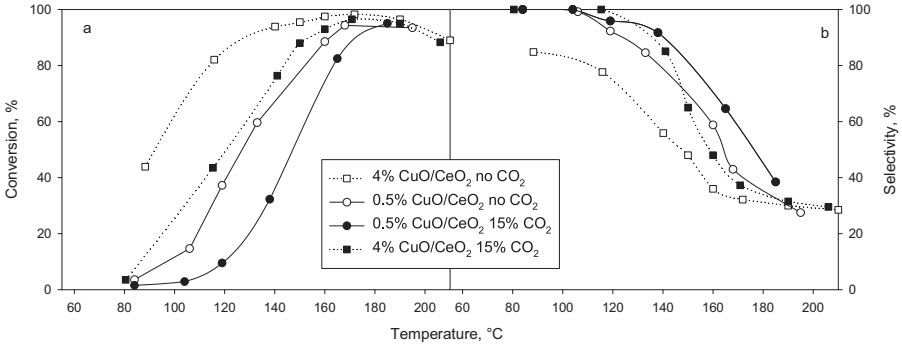

Fig. 4. CO conversion (a) and selectivity (b) as function of temperature as obtained over the 0.5% CuO/CeO_2 and 4% CuO/CeO_2 catalysts in the absence and in the presence of CO_2 (15%). $\tau = 0.054$ g s/cm^3; $CO/O_2/H_2 = 0.5/0.9/50$.

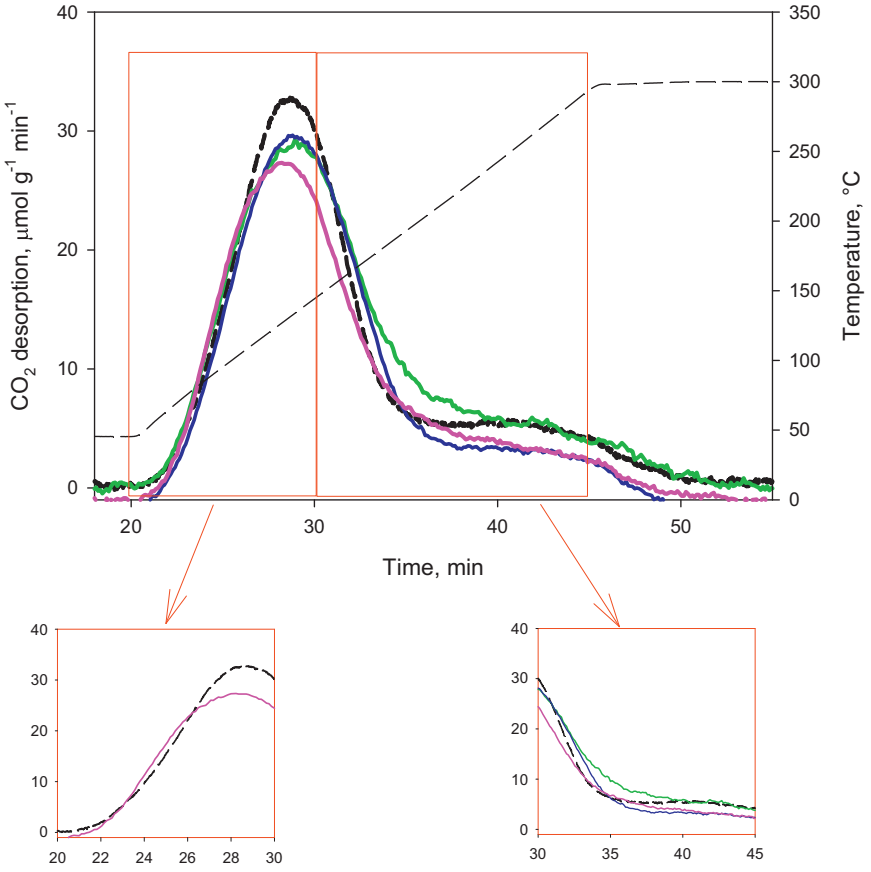

Fig. 5. TPD of CO_2 over CeO_2 and CuO/CeO_2 at different values of CuO content. (–) CeO_2; (—) 0.5% CuO/CeO_2; (—) 4% CuO/CeO_2; (—) 8% CuO/CeO_2. In the red boxes the enlargements of the TPD signals between 50 °C and 150 °C and between 150 °C and 300 °C respectively are reported.

In all cases a dominant CO_2 desorption signal is peaked at 120–135 °C whilst a smaller peak appears at 250 °C, more evident for the support. However, the CO_2 desorption shows a different behavior when copper is added to ceria. As highlighted in the left red box of Fig. 5, reporting the first part of TPD profiles of pure ceria and 4% CuO/CeO_2, in the presence of copper TPD signal shows a change of the slope not detectable on CeO_2. The other copper containing materials show the same behavior. In addition, also the approach to the valley point of the TPD patterns (right red box of Fig. 5) is different for support and copper containing materials, the first showing a faster decay.

The TPD curves shown in Fig. 5 are very similar to those reported by Avgouropoulos and Ioannides [29] for CuO-CeO_2 catalysts prepared by combustion synthesis although the values of CO_2 adsorption reported by Avgouropoulos and Ioannides [29] are always significantly smaller than those evaluated in this work, also considering the lower surface area of their samples. On the other hand, these values are higher than that relevant to the CO_2 desorbed in a CO TPD carried out over the same 4% CuO/CeO_2 catalyst [31]. The CO_2 detected in that experiment was addressed to the oxidation of a fraction of CO adsorbed to give CO_2 which is then desorbed by increasing temperature. Also the amount of CO adsorbed at room temperature [31] is lower than that of CO_2 suggesting that CO_2 interacts with a larger amount of surface sites compared to CO which is probably more selective towards copper sites and likely interacts with the support at lower extent.

This requires the development of an adsorption model which allows the identification of active sites which are inhibited by CO_2

Table 2
SRMSE values for all the catalysts investigated, as obtained for the two models tested.

Sample	2-site model	3-site model
0.5% CuO/CeO_2	0.02645	0.0207
4% CuO/CeO_2	0.0453	0.0305
8% CuO/CeO_2	0.0472	0.0326

adsorption although a possible spill-over of CO_2 from the support cannot be excluded during the CO-PROX reaction.

Finally, it must be pointed out that most of CO_2 (nearly 80% for the CuO/CeO_2 catalysts; 88% for the support) desorbs at temperature lower than about 180 °C. This supports the results of Fig. 3 confirming that in the second regime (Fig. 3, temperature higher than 160 °C) the CO_2 addition does not have any effect on both the CO conversion and selectivity.

3.3. Model results

In Fig. 6 the model curves are shown for each sample together with the experimental TPD profiles. The agreement is quite good up to about 230 °C. At higher temperature model results deviate from the experimental ones. The reason for this behaviour has been addressed to the baseline of the experimental device. Nevertheless, the temperature range of interest for the CO-PROX process is 80–200 °C.

To quantify the differences between the experimental and the model TPD curves we computed the root mean square error SRMSE normalized by the maximum value of the TPD curve (TPD_{max}):

$$\mathrm{SRMSE} = \frac{1}{\mathrm{TPD}_{\max}}\sqrt{\frac{1}{N}\sum_{i=1}^{N}(\mathrm{TPD\,exp}\,(i) - \mathrm{TPD\,exp}\,(i))^2} \qquad (23)$$

According to Kanervo et al. [32], if SRMSE ≤ 0.045 then the two curves may be considered in good agreement.

In the case of the support (CeO_2) we found the presence of only two sites (θ_1 and θ_2), while in the case of the copper catalyst (CuO/CeO_2) three sites are needed to reproduce the observed TPD profile (θ_1, θ_2 and θ_3). As a matter of fact, the model is able to reproduce better the TPD patterns of the catalyst when taking into account three different sites (3-site model) rather than two sites (2-site model). In Table 2 the values of SRMSE computed from the model TPD curves of the model with 2-site and with 3-site are given. It is worth noting that the model with two sites does not meet the criterion being the SRMSE value higher than 0.045. We also used the 3-site model to reproduce the TPD pattern of the support. In this case, the improvement of SRMSE is marginal and, consequently, the model to be chosen is that with the lower number of parameters.

In Table 3 the values of the kinetic parameters for the best models are given. From these values it turns out that the presence of copper oxide over the support surface significantly affects the activation energy of the CO_2 desorption rate of step 1 (θ_1). Indeed, the activation energy over the support is E_{a1} = 48,920 J/mol K while in the presence of CuO it decreases to 47,320 J/mol K. All the other kinetic parameters are not affected by both CuO addition and amount.

The lower value of the activation energy of step 1 (site θ_1) suggests that the θ_1 sites of the support (CeO_2) are energetically modified by the presence of CuO; as a consequence, it is reasonable to suppose that these sites are related to highly dispersed copper strongly interacting with the support, i.e. the Cu^{+2}—O^{-2}—Ce^{+4} species which are claimed as active centers for CO-PROX reaction [17–21].

In Fig. 6 the contribution of each site to CO_2 desorption is also plotted for all the samples. It is found that on increasing the CuO content, the contribution of site θ_1 decreases while the contribution of site θ_3 significantly increases. The high temperature contribution (θ_2) remains almost unaffected by the CuO amount.

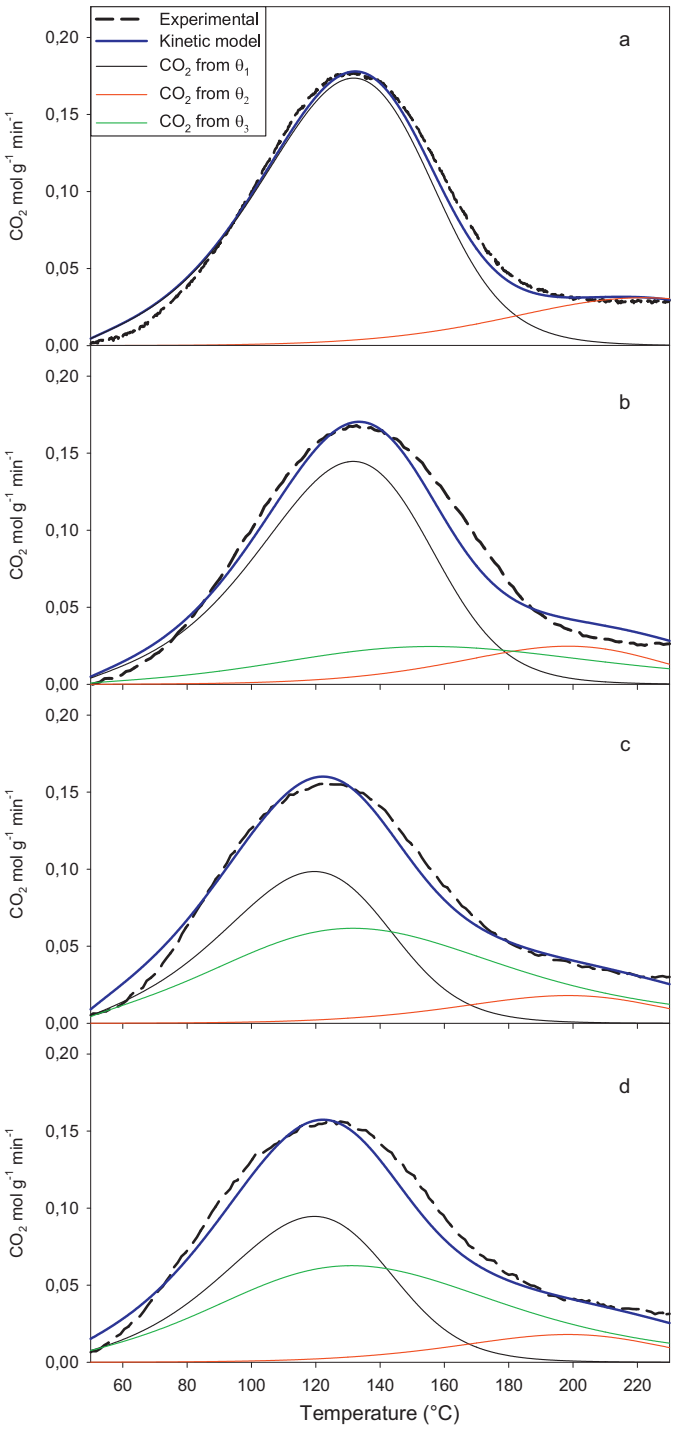

Fig. 6. Experimental (dashed lines) and modeling (solid lines) TPD of CO_2 over CeO_2 (a) and CuO/CeO_2 at different values of CuO content ((b) 0.5 wt.%; (c) 4 wt.%; (d) 8 wt.%). Carrier He, flow rate = 50 cm^3/min. Model CO_2 desorption curves from θ_1, θ_2 and θ_3 sites are also reported.

We computed the CO_2 amount initially adsorbed over the different sites of the catalyst from the initial values θ_1^0, θ_2^0 and θ_3^0 given in Table 3. In Fig. 7 these values are plotted as a function of the CuO content.

Sites θ_1, attributed to the support sites and to strongly interacting copper–ceria species, are those more significantly affected by copper coverage. Indeed, by increasing the CuO loading the amount

Table 3
Values of the kinetic parameters for the support and catalysts.

	θ_1^0	E_{des1} [a]	k_1^{0b}	n_1	θ_2^0	E_{des2} [a]	k_2^{0b}	n_2	θ_3^0	E_{des3} [a]	k_3^{0b}	n_3	SRMSE
CeO_2	0.66	48,920	1.1×10^6	1	0.16	51,500	1.4×10^5	1					0.038
0.5% CuO/CeO_2	0.55	48,900	1.1×10^6	1	0.11	51,500	1.4×10^5	1	0.18	39,034	1.0×10^5	2	0.0201
4% CuO/CeO_2	0.36	47,320	1.1×10^6	1	0.08	51,500	1.4×10^5	1	0.4	39,034	1.0×10^5	2	0.0305
8% CuO/CeO_2	0.35	47,320	1.1×10^6	1	0.08	51,500	1.4×10^5	1	0.41	39,034	1.0×10^5	2	0.0326

[a] $J\,mol^{-1}\,K^{-1}$.
[b] min^{-1}.

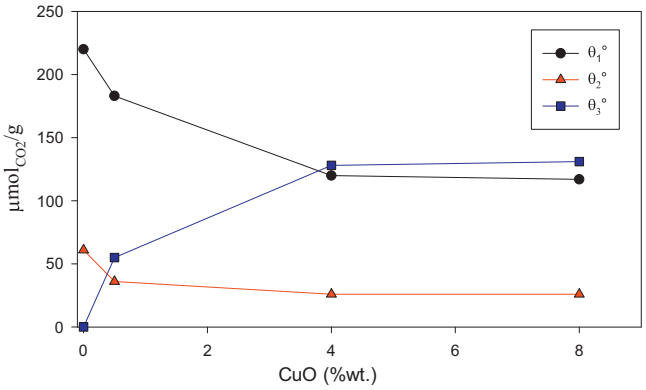

Fig. 7. Initial values of CO_2 amount adsorbed on sites 1, 2 and 3 as function of the CuO content.

of CO_2 adsorbed over θ_1 sites decreases up to 4 wt.% CuO suggesting that copper deposition partially covers these ceria sites not sufficiently balanced by new copper adsorption sites.

A further copper addition, exceeding the theoretical monolayer coverage (4 wt.% CuO), does not block the CO_2 access to these sites. The number of θ_2 sites (desorbing CO_2 at high temperature), also originally present on the support, slightly decreases by copper addition. On the contrary, θ_3 sites, not originally present on the support, increase with CuO loading and should be related to supported copper oxide. In contrast with Avgouropoulos and Ioannides [29] who found that CO_2 is desorbed from a high surface area bulk copper oxide at about 100 °C with a long tail up to 300 °C, a CO_2 TPD of pure tenorite CuO (not shown) provided a single narrow signal peaked at 278 °C with an area corresponding to 117 µmol CO_2 g^{-1}. This could suggest that particle dimension is strictly correlated to the strength of adsorption and, as a consequence, that a temperature of desorption of CO_2 from highly dispersed CuO particles cannot be unambiguously attributed. Indeed, the nature of supported copper oxide can be very different from that of bulk CuO and it is presumable that this kind of copper reaches the maximum amount approaching the monolayer coverage (i.e. 4 wt.% CuO). On the other hand, it was reported that also the catalytic activity did not increase by doubling CuO content (from 4 to 8 wt.%) [31] suggesting that the formation of bulk-like structures less interacting with ceria do not lead to higher CO conversion neither to a markedly greater CO_2 adsorption.

Finally, it should be noted that the reaction orders of the desorption rates from θ_1 and θ_2 sites are equal to 1 for each sample, suggesting that desorption from these sites are elementary steps. On the contrary, reaction order of the desorption rate from θ_3 sites is 2. In this case, our results suggest that CO_2 desorption from θ_3 sites is not elementary, but it probably needs two adjacent sites for CO_2 evolution into the gas phase.

In Fig. 8 the reaction rates of each step are plotted as a function of temperature as obtained for the catalysts and the support. It is shown that the reaction rates of each step of CO_2 desorption from the support is much higher than that from the catalyst. The reaction rates over the catalyst are the same but they are activated

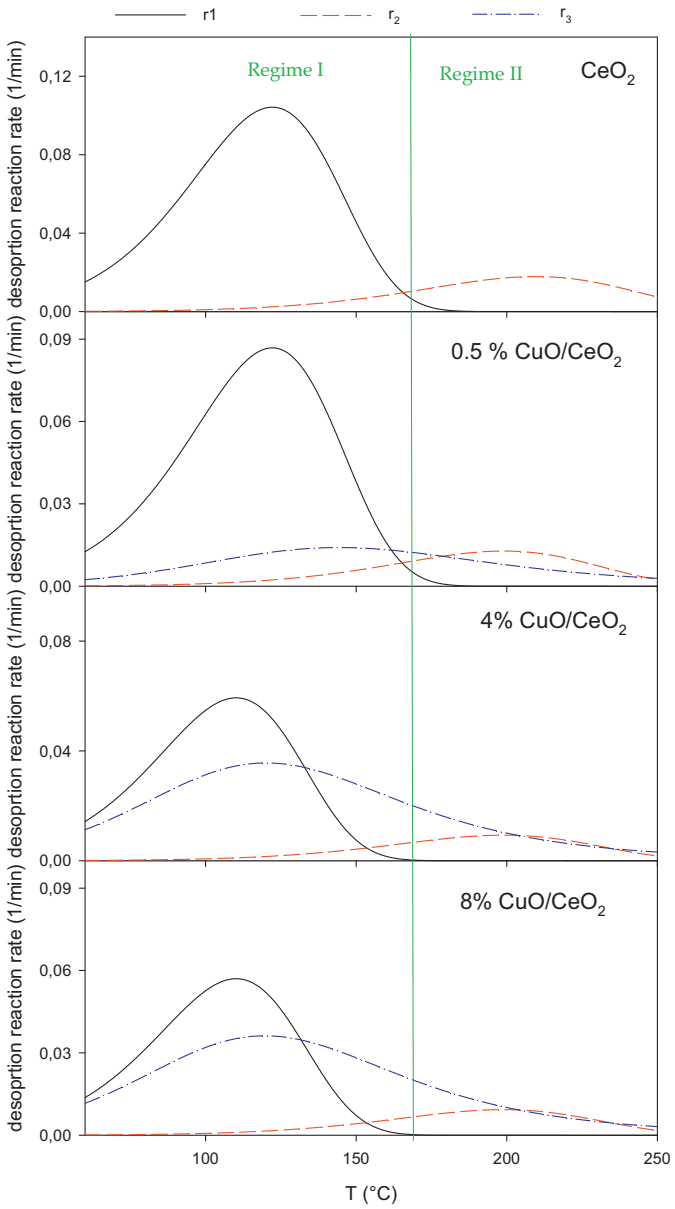

Fig. 8. Desorption reaction rates from CeO_2 and CuO/CeO_2 (0.5, 4 and 8 wt.%) as function of temperature as computed by the model.

at different temperatures. Conversely, in the support a dominant reaction step (step 1) is found while the desorption reaction rate from site 2 (θ_2) is much lower.

In Fig. 9 the catalyst coverage (θ_1, θ_2 and θ_3) are plotted as a function of temperature as obtained for all the samples investigated.

From the results of Figs. 8 and 9 two different regimes may be identified. In Regime I ($T < 160$ °C) CO_2 is completely desorbed from site 1 (θ_1) while it still remains adsorbed over sites 2 and 3.

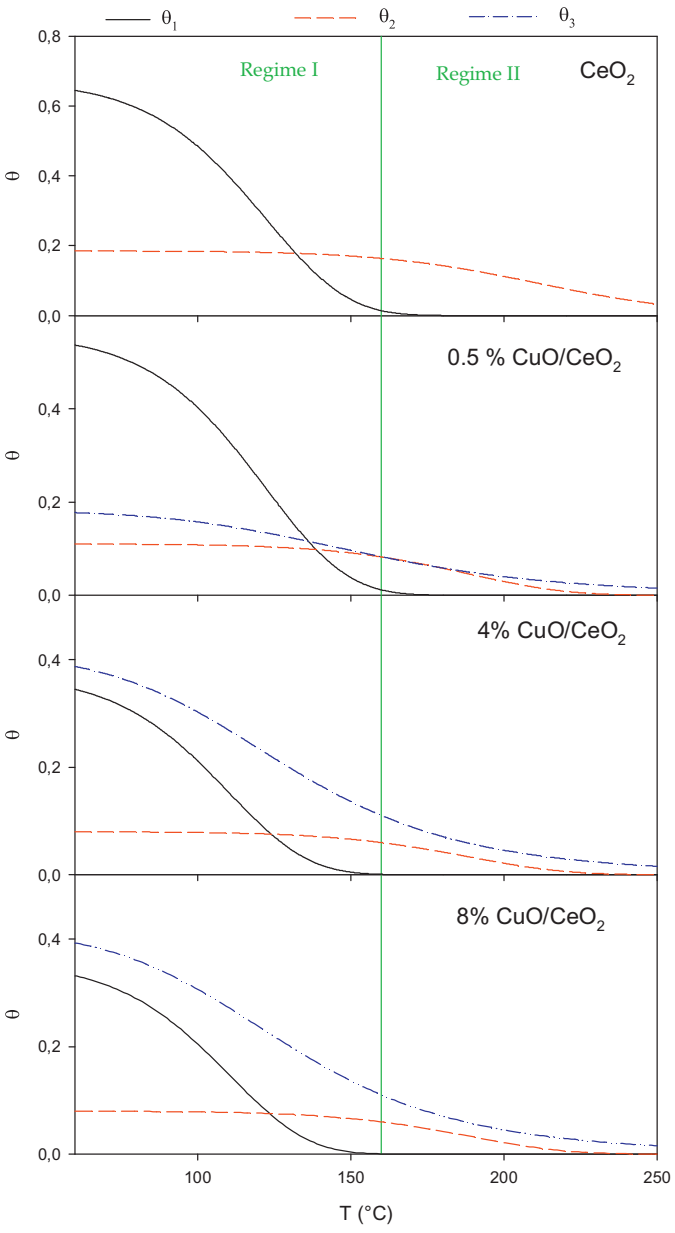

Fig. 9. CO_2 adsorbed sites over CeO_2 and CuO/CeO_2 as function of temperature as computed by the model.

At temperature higher than 160 °C (Regime II) CO_2 starts desorbing also from site 3, while CO_2 desorption from site 2 occurs at very high temperature values outside from the CO-PROX activity temperature range.

As a consequence, we may conclude that the θ_1 sites should be significantly involved in the CO oxidation while most part of θ_3 sites are probably active toward the H_2 oxidation. These results support the conclusion of Lee and Kim [26] who proposed that CO and H_2 oxidation occurs over two different active sites: Cu^+-carbonyl sites are active for CO oxidation while Cu^0 sites for H_2 oxidation. In addition, the CO_2 adsorption model proposed allowed us to assign different CO_2 adsorption properties to the different active copper sites.

On the basis of the above considerations we can also identify the region corresponding to the last part of the Regime I (Fig. 3) as an optimal operating zone (temperature: 140–160 °C) under CO_2-rich mixtures. Indeed, under these conditions copper sites devoted to H_2 oxidation (θ_2) are still significantly occupied by chemisorbed CO_2, while the most part of copper sites related to CO oxidation (θ_1) are CO_2-free. This leads to a higher CO yield compared to that obtained under CO_2-free conditions in the same temperature range due to a comparable CO oxidation performance but to a lower detrimental H_2 oxidation activity at the same time.

In conclusion, the CO_2 desorption model proposed in this work provides a qualitative and quantitative analysis of sites involved in CO_2 chemisorption also suggesting a condition of surface coverage where sites associated to H_2 oxidation are selectively blocked.

4. Conclusions

The inhibiting effect of carbon dioxide on the CuO/CeO_2 activity towards CO-PROX reaction has been studied. CO_2 reduces the catalytic activity but increases the CO selectivity at temperatures below 160 °C, while at higher temperatures catalytic performance appears unaffected by CO_2 co-feeding. As highlighted by TPD experiments, CO_2 is chemisorbed onto both the ceria support and CuO/CeO_2 catalysts, thus suggesting that its inhibiting effect is due to the formation of stable surface species. By modeling of TPD profiles, two adsorption sites on the ceria support and an additional one on copper containing materials have been identified.

The low temperature site is energetically modified by copper addition, thus suggesting the attribution to Cu^{+2}—O^{2-}—Ce^{+4} species, claimed as CO oxidation sites. CO_2 is completely desorbed from these sites at about 160 °C, thus confirming that these species are those active towards CO oxidation. Otherwise, sites exclusively related to copper desorbed CO_2 at temperatures slightly higher. These sites should be mainly responsible for H_2 oxidation, thus explaining the increased CO selectivity in a wide range of temperature.

Acknowledgements

This work was financially supported by MIUR (FIRB2010 “Futuro in Ricerca”).

References

[1] E.G. & G. Technical Services, Inc., Fuel Cell Handbook, seventh edition, 2004, http://www.netl.doe.gov/technologies/coalpower/fuelcells/seca/pubs/FCHandbook7.pdf
[2] H. Iragashi, H. Uchida, M. Suzuki, Y. Sasaki, M. Watambe, Applied Catalysis A 159 (1997) 159–169.
[3] M.M. Schubert, S. Hackenberg, A. van Veen, M. Muhler, V. Plzak, R.J. Behm, Journal of Catalysis 197 (2001) 113–122.
[4] M.M. Schubert, V. Plzak, J. Garche, R.J. Behm, Catalysis Letters 76 (2001) 143–150.
[5] O. Korotkikh, R. Farrauto, Catalysis Today 62 (2000) 249–254.
[6] G. Avgouropoulos, T. Ioannides, Applied Catalysis B: Environmental 67 (2006) 1–11.
[7] I. Lopez, T. Valdes-Solis, G. Marban, International Journal of Hydrogen Energy 33 (2008) 197–205.
[8] G. Avgouropoulos, T. Ioannides, H. Matralis, J. Batista, S. Hocevar, Catalysis Letters 73 (2001) 33–40.
[9] T. Caputo, L. Lisi, R. Pirone, G. Russo, Industrial and Engineering Chemistry Research 46 (2007) 6793–6800.
[10] A. Martinez-Arias, A.B. Hungria, G. Munuera, D. Gamarra, Applied Catalysis B 65 (2006) 207–216.
[11] W. Liu, M. Stephanopoulos, Journal of Catalysis 153 (1995) 304–316.
[12] W. Liu, M. Stephanopoulos, Journal of Catalysis 153 (1995) 317–332.
[13] S. Hocevar, U.O. Krasovec, B. Orel, A. Arico, H. Lim, Applied Catalysis B 28 (2000) 113–125.
[14] H. Zou, X. Dong, W. Lin, Applied Surface Science 253 (2006) 2893–2898.
[15] A. Martínez-Arias, A.B. Hungría, M. Fernández-García, A. Iglesias-Juez, J. Soria, J.C. Conesa, J.A. Anderson, G. Munuera, Physical Chemistry Chemical Physics 14 (7) (2012) 2144–2151.
[16] D. Gamarra, C. Belver, M. Fernández-García, A. Martínez-Arias, Journal of the American Chemical Society 129 (40) (2007) 12064–12065.
[17] A. Martinez-Arias, M. Fernandez-Garcia, O. Galvez, J.M. Coronado, J.A. Anderson, J.C. Conesa, J. Soria, G. Munuera, Journal of Catalysis 195 (2000) 207–216.
[18] G. Sedmak, S. Hocevar, J. Levec, Journal of Catalysis 213 (2003) 135–150.

[19] W. Shan, W. Shen, C. Li, Chemistry of Materials 15 (2003) 4761–4767.
[20] M. Manzoli, R. Di Monte, F. Boccuzzi, S. Coluccia, J. Kaspar, Applied Catalysis B: Environmental 61 (2005) 192–205.
[21] G. Marban, I. Lopez, T. Valdes-Solis, Applied Catalysis A-General 361 (2009) 160–169.
[22] J.L. Ayastuy, A. Gurbani, M.P. Gonzalez-Marcos, M.A. Gutierrez-Ortiz, International Journal of Hydrogen Energy 35 (2010) 1232–1244.
[23] S.H. Oh, M.R. Sinkevitch, Journal of Catalysis 142 (1993) 254–262.
[24] F. Marinõ, C. Descorme, D. Duprez, Applied Catalysis B: Environmental 58 (2005) 175–183.
[25] D. Gamarra, A. Martínez-Arias, Journal of Catalysis 263 (2009) 189–195.
[26] H.C. Lee, D.H. Kim, Catalysis Today 132 (2008) 109–116.
[27] R. Kydd, D. Ferri, P. Hug, J. Scott, W.Y. Teoh, R. Amal, Journal of Catalysis 277 (2011) 64–71.
[28] J.W. Park, J.H. Jeong, W.L. Yoon, Y.W. Rhee, Journal of Power Sources 132 (2004) 18–28.
[29] G. Avgouropoulos, T. Ioannides, Catalysis Letters 116 (2007) 15–22.
[30] T. Caputo, R. Pirone, G. Russo, Kinetics and Catalysis 47 (2006) 756–764.
[31] T. Caputo, L. Lisi, R. Pirone, G. Russo, Applied Catalysis A – General 348 (2008) 42–53.
[32] J.M. Kanervo, T.J. Keskitalo, R.I. Slioor, A.O.I. Krause, Journal of Catalysis 238 (2006) 382–393.